

Realism in Action: Anomaly-Aware Diagnosis of Brain Tumors from Medical Images Using YOLOv8 and DeiT

Seyed Mohammad Hossein Hashemi ^{a,*}, Leila Safari ^a, Amirhossein Dadashzadeh Taromi ^b

^a Department of Computer Engineering, Faculty of Engineering, University of Zanjan, Zanjan, 45195-313, Iran

^b Department of Computer Science and Information Technology, Institute for Advanced Studies in Basic Sciences, Zanjan, 45137-66731, Iran

* Corresponding author.

E-mail address: 1mohammad0hossein1@gmail.com (S.M.H.Hashemi)

ABSTRACT

In the field of medical science, the reliable detection and classification of brain tumors from images remain a formidable challenge due to the rarity of tumors within the patient population. The ability to detect tumor cases in anomaly scenarios is paramount for ensuring timely interventions and improved patient outcomes. This study addresses this challenge by leveraging deep learning (DL) techniques to detect and classify brain tumors in challenging situations. This study employs deep learning (DL) techniques to address this challenge, utilizing a dataset from the National Brain Mapping Lab (NBML) comprising around 30,000 slices belonging to 81 patients, including 30 tumor cases and 51 normal cases. Our approach consists of two phases: detection and classification. In the first phase, extensive data pre-processing simulated real-world conditions, adjusting the dataset to reflect an anomaly distribution of 9 normal cases for every 1 tumor case. Next, a YOLOv8n model was fine-tuned to detect tumor regions. To assess the model's performance at the patient level, we introduced the Patient-to-Patient (PTP) metric, which evaluates the ability to identify tumor cases across an entire population rather than measuring the performance for individual slices. This approach provides a more clinically relevant evaluation of model reliability. The model achieved F1-score of 0.98 and PTP-F1-Score of 1.0, correctly classifying all the patients within the testing population. In the classification phase, the Data Efficient Image Transformer (DeiT) was used to distill a Vision Transformer (ViT) model from a ResNet152 teacher model. DeiT was selected for its ability to train effectively on small datasets. The distilled classifier achieved F1-score of 0.92 after 20 epochs, while the ResNet152 model achieved 0.97, albeit with higher computational costs. This study demonstrates notable advancements in the reliable detection and classification of brain tumors in challenging situations, offering a potential for practical applications.

Keywords:

Anomaly distribution, Brain tumors, Tumor diagnosis, Medical imaging, ResNet152, Vision Transformer, YOLOv8n.

1. Introduction

Reliability and precision are pivotal factors in the context of brain tumor diagnosis. The brain, a vital organ situated within the human body that oversees the entire nervous system [1]. Consequently, any deviations within the brain can significantly impact human health. Among these anomalies, brain tumors stand out as particularly severe. Brain tumors involve the uncontrolled and aberrant growth of cells within the brain. These tumors can be categorized into two groups: primary tumors and secondary tumors. Primary tumors emerge within the brain tissue itself, whereas secondary tumors

stem from other areas of the body, migrating to the brain tissue through the bloodstream [2]. Glioma and Meningioma are two severe types of brain tumors among primary tumors. If not identified in their early stages, these tumors can lead to fatal outcomes for patients [3].

In the context of the detection and monitoring of brain tumors, nowadays, with huge advancements in the medical imaging field, there are various imaging technologies used by radiologists and doctors to observe internal human body organs, such as computed tomography (CT), positron emission tomography (PET), and magnetic resonance imaging (MRI). Among the array of modalities available, MRI emerges as the foremost selection for non-invasive brain tumor detection and evaluation. This preference is owed to its remarkable resolution and superior ability to provide contrasting details of soft tissues [4]. Manually scrutinizing these images is a laborious and demanding endeavor. Moreover, it is susceptible to errors, particularly given the surge in patient volumes and the relatively low incidence rate of brain tumors [5], [6]. This combination makes detecting and categorizing these tumors a formidable challenge. In response, our objective is to formulate a resilient, anomaly-conscious, computer-aided, automated solution. This approach aims to enhance the accuracy of clinical brain tumor diagnosis.

The initial challenge in the study of tumor diagnosis lies in the significant variability of tumors in terms of their shapes, textures, and contrasts, both within and between cases [7]. Within the realm of tumor diagnosis, scientists have harnessed a diverse array of deep learning algorithms. They employed a diverse array of methods, including VGGNets [8], GoogleNet [9], and ResNets [10]. These advanced algorithms have been instrumental in assisting with tumor diagnosis. However, these models often rely on semi-balanced datasets gathered from balanced populations, which may not reflect the true clinical scenarios where non-tumor cases vastly outnumber tumor cases.

In this regard, based on the most recent statistical data released by Johns Hopkins Medicine, the incidence rate of brain and nervous system tumors in the United States is approximately 30 adults per 100,000 individuals [6]. Indeed, the incidence rate can differ significantly based on age, gender, location, and other population factors. However, a thorough review of recent data suggests that this number remains very low. Although the rare occurrence of this illness is comforting, difficulties arise when doctors need to identify these uncommon cases in a large and diverse populations [11].

In this study, we proposed a deep learning-based solution trained and evaluated in scenarios closely resembling clinical diagnoses. Unlike previous studies, our method introduces a unique approach to training a model that not only detects and classifies each image into its corresponding class but also makes classifications regarding each patient's overall diagnosis. This unique perspective could help to address the challenges posed by the low incidence of brain tumors by introducing a robust model and offering a new method of performance evaluation. Furthermore, it could illuminate a path toward designing a fully autonomous decision-making system for brain tumor diagnosis.

Our solution utilizes two key factors:

Firstly, (1) we harness a substantial quantity of distinct image data from the data set we acquired from NBML. This data set encompasses records from 81 patients who underwent monitoring using various imaging technologies, such as CT, PET, and MRI.

Secondly, (2) we implement a meticulous data preprocessing pipeline. This pipeline not only refines the data set to skew its distribution towards non-tumor samples but also preserves category proportions while augmenting data within each class, thus enhancing overall sample diversity.

In the tumor detection phase, we trained the YOLOv8n model on our data set to yield accurate yet anomaly-resistant detections. Subsequently, we proceed to the evaluation phase, where we gauge the model's efficacy in tumor detection. This assessment employs novel PTP evaluation functions beside common metrics, providing a pragmatic understanding of the model's performance during execution by capturing its performance in identifying tumor cases among the patients population.

Next, we utilized a distilled ViT using the DeiT architecture with a fine-tuned ResNet152 as the teacher model [12]. We incorporated this model for its attention mechanism and the lightness, features that are crucial for practical implementations. This model contributes to classifying brain tumor types into three distinct classes: Meningioma, Pituitary, and Glioma.

The following paragraphs are structured as follows: Section II is a literature review on related works in this field, Section III explains the materials and methods we utilized, Section IV presents the results we achieved, and Section V concludes the article.

1.1 Related Works

Following the advancements of ML algorithms, many valuable contributions have been made to offer robust and accurate solutions for the brain tumor classification problem [13–15]. Kang et al. [7] proposed a pipeline that combines CNN pre-trained models, such as ResNet, DenseNet, and VGG, to extract features from MRI images and evaluate them using various ML classifiers like Random Forest and SVM. By creating a distinctive feature vector through bagging and classifier combination, they enhanced classification accuracy. However, this approach heavily relies on feature engineering, which may limit its applicability in more general settings and does not directly address the issue of class imbalance in datasets.

During the last decade, computer hardware advancements, especially Graphical Processing Units (GPU), have caused DL solutions to be an undeniable and consistent solution for many tasks. In this regard, various CNN-based architectures (e.g., DenseNets, Xception, VGG-Nets, etc.) have been introduced for image processing tasks, and many of them have been applied to studying brain tumor classification [16–27].

Ahmad et al. [28] proposed a framework based on unsupervised deep generative neural networks that combine Variational Auto Encoders (VAEs) and Generative Adversarial Networks (GANs) to generate realistic brain tumor MRIs. The proposed method significantly improves the performance of the ResNet50 classifier, achieving an average accuracy improvement from %72.63 to %96.25. This method shows great potential as a clinical tool due to its high accuracy, but the complexity and computational demands of generative models could be a limitation in practical applications.

Sharif et al. [29] proposed a method utilizing DenseNet201 pre-trained on imbalanced data. The model extracts features from the average pool layer but claims this alone is insufficient for reliable classification. To address this, two feature selection techniques are introduced: Entropy-Kurtosis based High Feature Values (EKbHFV) and a Modified Genetic Algorithm (MGA), further refined by a threshold function. These selected features are fused using a non-redundant serial approach and classified by a multi-class SVM cubic classifier, achieving 95% accuracy. However, the reliance on complex feature selection reduces its generalizability across diverse datasets. While this method achieved significant accuracy, the reliance on complex feature selection techniques introduces additional complexity and may not be easily generalizable across different datasets.

Asiri et al. [30] developed a model called a fine-tuned Vision Transformer (FT-ViT), achieving high accuracy in brain tumor classification tasks. While the use of ViT models is effective due to their ability to handle complex image structures, the extensive training time required and the computational demands for real-time deployment pose significant challenges for practical medical applications. To address these issues, we employed a Data Efficient Image Transformer (DeiT) approach to distill the knowledge from a large ResNet152 model into a more compact ViT. This process allowed us to significantly reduce computational requirements, making the ViT more efficient and suitable for resource-constrained clinical environments. This approach, while slightly reducing accuracy, strikes a balance between performance and practical usability in real world medical settings.

Tummala et al. [31] discusses using an ensemble of pretrained ViT models to classify brain tumors from MR images. They evaluated an array of ViT models and analyzed their performance on brain tumor classification tasks. They concluded that the best model among the pretrained ViT models is L/32, with an overall test accuracy of %98.2. However, they added that when all four ViT models are ensembled together, the accuracy improves to %98.7. This approach benefits from the combined strengths of multiple models, but the increased complexity and resource demands associated with ensemble learning may pose challenges for implementation.

Abdusalomov [32] enhanced the YOLOv7 model by incorporating a Convolutional Block Attention Module (CBAM) and Spatial Pyramid Pooling Fast+ (SPPF+) layers, which improved the model's accuracy in detecting brain tumors to 99.5%. While this enhancement demonstrates notable improvement in detection accuracy, the study only measures the performance of the model in relatively unrealistic population and does not address the issue of inherent class imbalance.

Unlike previous studies, which often assume balanced datasets and do not fully address the challenges of low incidence rates of tumors, our work specifically focuses on these aspects. We introduced a novel Patient to Patient (PTP) metric to assess not only image-level detection but also patient-level diagnostic reliability. This innovation highlights the practical implications of our work, providing a robust framework for tumor diagnosis in challenging clinical environments.

2. Materials and Methods

In this section, we explain the steps we took for data preparation and then elaborate our proposed framework for tumor detection and classification. Our general approach here is to break down the complex task of tumor diagnosis into smaller sub-problems.

Accurate brain tumor diagnosis involves two distinct goals: 1. Detecting tumors within a predominantly Normal dataset, and 2. Identifying unusual brain tissues and their type from their unique characteristics in highly noisy scenes (e.g., shape and suspicious tissue placement).

The first phase of our framework, tumor detection, focuses on addressing the first goal, which is training a model that is resilient to anomaly-distributed populations and can accurately detect brain tumors in various imaging modalities.

The second phase of our framework, tumor classification, involves through data collection and preparation steps to merge multiple publicly available datasets into a single source of data and convert them into a suitable format for the classifier. Next, we created a custom DeiT model and trained it to classify brain tumors in three classes of Meningioma, Pituitary, and Glioma.

2.1 Brain Tumor Detection

This phase includes comprehensive data collection from private data sources and unique pre-processing steps to mimic realistic tumor diagnosis scenarios. In this regard, we collected a relatively small image dataset of Normal and Tumor classes with samples belonging to 81 patients, with 30 being Tumor cases and 51 Normal. Next, we subjected the dataset to a custom method of data pre-processing that included data distribution modification techniques and data augmentation, to transform the dataset into a suitable format.

Coming to the next step, we trained and fine-tuned the YOLOv8n model for the tumor detection task. Furthermore, during the evaluation step, in addition to common evaluation metrics we employed a novel PTP evaluation function to facilitate a pragmatic assessment of the model's performance.

Figure 1 depicts the proposed brain tumor detection procedure. As it is shown in the figure, the raw data passes through a data pre-processing pipeline and transformed into a suitable format for the detection model, the YOLOv8n. Based on the model's prediction, the tumor-detected samples are fed into the classifier for tumor type classification. The details of the sub-components of Figure 1 are explained in the following subsections.

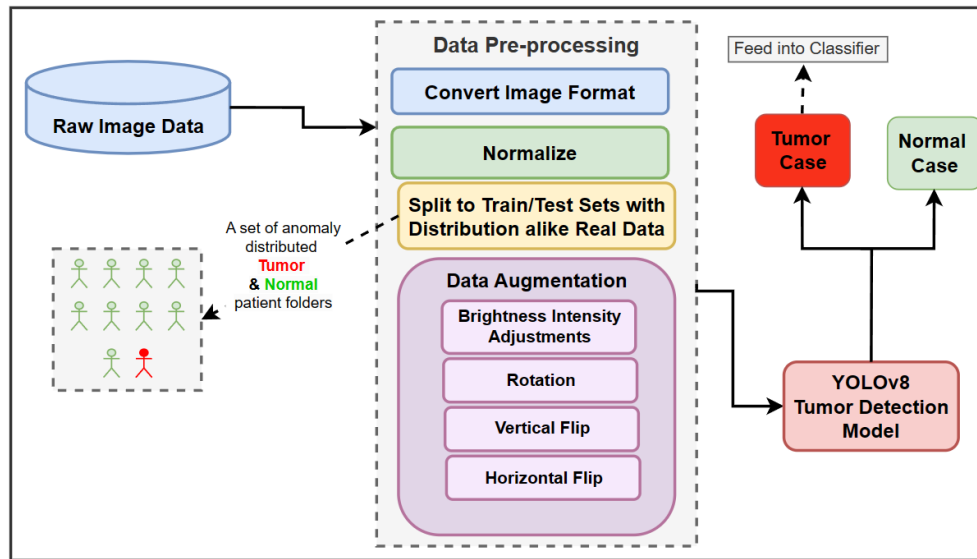


Fig. 1. Brain Tumor Detection Process.

2.2 Data Collection

During the training phase of our brain tumor detection model, we utilized a dataset from the National Brain Mapping Lab (NBML), comprising 81 patients—30 with confirmed brain tumors and 51 classified as normal. Each patient's dataset contained multiple medical imaging modalities, including PET, CT, and MRI scans. The MRI data consisted of 2D images captured through T1-weighted, T2-weighted, and diffusion-weighted sequences. Consequently, we assert that the data set inherently incorporates a form of data augmentation. In simpler terms, the inclusion of diverse imaging modalities for each patient mitigates the potential for bias towards any particular modality, such as MRI. Importantly, it is imperative to emphasize that the data set obtained from NBML has been

exclusively employed for the detection phase and it is held privately, with all associated rights and credits attributed to Iranian Brain Mapping Biobank (IBMB) resources.

2.3 Data Pre-processing

The essence of our data preparation pipeline centers on the careful pre-processing of our data set to closely mirror real-world scenarios. In this section, we will explain the first critical aspect of our methodology, which is distributing the patient data to ensure it reflects real-world scenarios for testing. In section D, we will outline the specific steps we took to determine the threshold for classifying patients into their corresponding classes.

In the context of brain tumors, the United States typically reports [33] incidence rates ranging from 0.03 to 0.06. We recognize that other nations may experience different rates due to their distinct factors. Given the limitations stemming from our limited dataset for the detection phase and the absence of comprehensive external data sources, we exercised caution by adopting a conservative estimate of a 0.1 incidence rate. The decision was made to simulate the anomalous scenario of detecting a Tumor case from Normal cases. Subsequently, following our presumed brain tumor distribution in the general population, we segmented the data set into two sets: one for training and the other for testing, with a particular stipulation. Specifically, in the training data set, we ensured that there were nine randomly selected Normal images for every tumor image. This approach was rooted in our hypothesis that, throughout both the training and evaluation phases, the model's focus should not lie in discerning each individual's situation but rather in acquiring knowledge from a diverse spectrum of patients exhibiting various scenarios and learning more robust and distinctive features.

Moving on to the testing set, we specifically selected 30 patients, encompassing 27 cases categorized as Normal and 3 cases as Tumor, with their corresponding folders housing all associated images. We aimed to maintain a distribution of Tumor and Normal patients that closely aligns with real-world scenarios while upholding the distribution pattern established during training. Notably, this step presented a primary challenge as each patient possessed a varying number of images, and the initial data set distribution significantly diverged from our desired goal. Additionally, we had to address the issue of particular images from tumor patients not exhibiting any signs of brain tumors, necessitating their removal and cleansing from the training data set.

To address the challenges at hand, we followed a systematic approach as below:

1. Utilizing a third-party software (MicroDicom) to convert DICOM-format patient folders and their associated images into “.png” format, standardizing their resolution to 540x540 pixels. Our initial data examination revealed approximately 18,000 Normal images distributed among 51 patients, while around 30 Tumor patients contributed roughly 12,000 image samples.
2. Resizing all images to a uniform size allowed us to compress each patient's folder into a ZIP archive, providing a precise count of images per patient and facilitating the selection process for each data set section.
3. Prioritizing data preservation and efficiency for the testing set, opting for the 27 normal patient folders with the smallest ZIP file sizes, resulting in 27 patients.

4. Choosing the three files with the smallest ZIP sizes from the uncleaned tumor patient folders. Ending up with a total of 30 patients for the testing set, achieving a tumor case distribution rate of 10%.
5. Selectively picking the remaining cleaned tumor case folders to construct our training set, and including approximately 1.4k tumor-indicative images, supplemented by 12,000 normal samples. This created an intentionally skewed training data set with a tumor-to-normal sample distribution of 10%, meaning we assigned nine normal images for each tumor image.
6. To enhance the diversity of our training samples and proactively mitigate the risk of overfitting while having more control over the data preparation process, we developed a tailored data augmentation class utilizing Python's built-in libraries. This augmentation class encompassed modifications such as brightness intensity adjustments, rotations, as well as vertical and horizontal flips, all while ensuring the corresponding bounding boxes (the rectangular area indicating the tumor tissue) were appropriately adjusted. The execution of the data augmentation pipeline has led to a substantial expansion in the overall data set volume, all while preserving its initial distribution. This augmentation procedure has contributed to enhancing and diversifying our training data, resulting in an overall improvement in data quality.

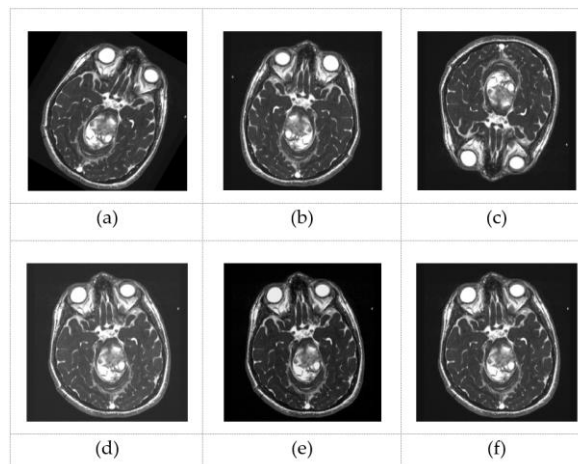


Fig. 2. Outputs of the augmentation module for a random 2D MRI sample. (a) Rotated sample; (b) Horizontally flipped sample; (c) Vertically flipped sample; (d) Brightened sample; (e) Dimmed sample, (f) Normal sample.

2.4 Proposed PTP Evaluation Metrics

In our research, our primary goal is to improve the model performance in real-world situations compared to academic assessments. To achieve this, we have introduced a new evaluation method called PTP. In this methodology, instead of indiscriminately feeding MRI images into the model without considering their patient origins, we adopt a more pragmatic strategy: feed in all the MRI scans from each patient. The model then carefully examines each image for any signs of abnormalities related to brain tumors. It keeps track of the number of images showing these signs, and if this count goes above a certain threshold, the model classifies the case as indicative of a tumor. So, instead of relying solely on standard evaluation metrics like F1-Score, Recall, Precision, and Accuracy, we have adopted a PTP-based evaluation metrics.

The PTP-based evaluation metrics are implemented as a straightforward Python function that systematically iterates through each patient's directory within the testing data set. Within this process, it feeds the images specific to each patient into the model for analysis. While the model processes each image individually and generates corresponding predictions, the PTP function maintains a record of these predictions. After completing this iterative procedure and analyzing all images within a patient's folder, the PTP function calculates a patient-specific tumor threshold. This threshold represents the proportion of images indicative of tumors within the entire collection of a patient images. If this computed threshold surpasses the predefined General Tumor Threshold (GTT), the PTP function classifies the patient as a Tumor case. This process is repeated individually for each patient, with the PTP function iterating through all patients in the dataset. Ultimately, the PTP function computes additional metrics, encompassing PTP-ACC, PTP Recall, PTP-Precision, and PTP-F1. It is noteworthy that this function is designed and deployed only as an evaluation metric for the Tumor detection model; hence, during the classification phase, we utilized common evaluation metrics such as accuracy to assess the model. Here is a concise explanation of the mentioned metrics:

- **PTP-ACC:** This metric assesses the model's accuracy in classifying patients as having tumors or not based on their individual tumor thresholds. This metric quantifies the proportion of correctly identified patient cases in the total patient population. In essence, it measures how well the model can distinguish patients with tumors from those without, providing a valuable indicator of its overall accuracy in patient classification.
- **PTP-Recall:** This metric evaluates the model's ability to correctly identify patients with tumors among all individuals who genuinely have tumors. It quantifies the ratio of true positive patient cases (those correctly identified as having tumors) to the total number of patients with tumors in the data set. PTP-Recall is a crucial measure of the model's sensitivity, highlighting its effectiveness in capturing all patients with tumors and minimizing the risk of missing any cases.
- **PTP-Precision:** This metric gauges the precision of the model in labeling patients as having tumors, considering the instances it has identified as positive cases. It calculates the ratio of true positive patient cases to the total number of patient cases labeled as having tumors by the model. This metric provides insights into the model's precision in patient classification, emphasizing its ability to minimize false positive identifications while maintaining accuracy.
- **PTP-F1:** This metric combines the metrics of PTP-Precision and PTP-Recall into a single score to offer a balanced evaluation of the model's performance in identifying patients with tumors. Calculated as the harmonic mean of these two metrics, PTP-F1 takes into account both false positives and false negatives in patient classification. This is particularly valuable when there is an imbalance between the number of patients with and without tumors, as it provides a comprehensive assessment of the model's overall performance.

2.5 General Tumor Threshold

An essential preliminary step in deploying the PTP function is the determination of the GTT applied uniformly across the patient population. The GTT is defined as the threshold value representing the proportion of images the model must classify as indicative of tumors within all the images belonging to a patient to designate it as a tumor case. To establish this threshold, we adopted an approach wherein we provided the entire patient data set, comprising patients from the training and validation sets, in

its original format and fed it into the trained model. Subsequently, we allowed the PTP function to calculate the number of tumor-indicative images per patient across the entire training and validation sets. Based on those values, we picked a suitable yet reliable GTT threshold value. The details of the GTT calculation further explained in the results section.

2.6 Detection Model

The YOLO (You Only Look Once) series, developed by Ultralytics, has become prominent in the field of computer vision, particularly in real-time object detection. YOLO models are valued for their balance between accuracy, speed, and model compactness, making them ideal for deployment in resource-constrained environments. The latest iteration, YOLOv8, continues to build on these strengths, offering architectural enhancements that significantly improve performance across a wide range of tasks, including object identification, image categorization, and segmentation.

2.7 Rationale for Choosing YOLOv8 over other Models

a) Performance in Complex Scenarios:

YOLOv8's architectural enhancements, such as its advanced backbone and neck modules, significantly improve its performance in detecting objects in complex and noisy environments, which is essential for identifying anomalies like tumors in medical images [34].

b) Generalization and Versatility:

In the context of medical imaging, the ability to generalize from limited datasets is crucial due to privacy concerns and the difficulty in acquiring large amounts of annotated data. YOLOv8's effectiveness in training on small datasets and leveraging transfer learning with pre-trained weights makes it particularly well-suited for medical applications [35]. This stands in contrast to models like ViTs, which, while powerful in handling large-scale data, can be less efficient with smaller datasets or require extensive data augmentation to achieve similar results [36].

Furthermore, Region-based Convolutional Neural Networks (R-CNN), although highly accurate, often involve complex region proposal steps that make them computationally expensive and slower compared to YOLOv8. YOLOv8's end-to-end training pipeline, which does not require separate region proposal networks, offers a significant advantage in terms of both training time and inference speed, making it more practical for real-world medical applications where quick decision-making is essential [37].

c) Proven Performance in Object Detection Benchmarks:

The YOLO family has consistently demonstrated strong performance in medical applications [35]. In our study, we selected YOLOv8n as the backbone model for tumor detection after evaluating its performance across different YOLO versions, as illustrated in Fig. 3. YOLOv8n exhibited substantial improvements in speed and accuracy compared to its predecessors (YOLOv5 to YOLOv7), making it the ideal choice for our anomaly-aware diagnosis system. The model's efficiency was further enhanced

by fine-tuning it on our purposefully skewed dataset, which better reflects real-world anomaly distributions.

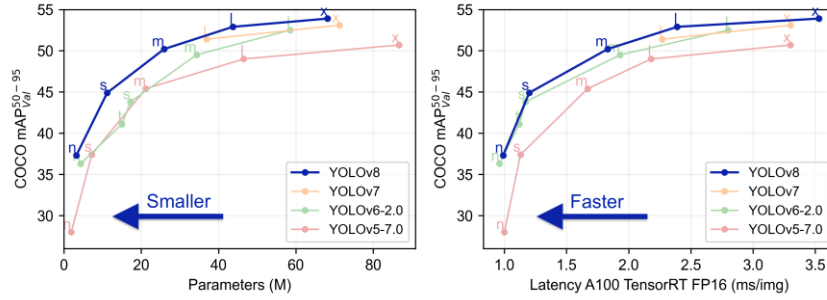


Fig. 3. YOLO Models Evaluation results compared based on COCO mAP (higher is better) [38]

Furthermore, YOLOv8's use of distributional focal loss, which treats box locations as probability distributions, provides a more nuanced approach to object detection, especially beneficial in medical imaging where precision is paramount. Given these advantages, we determined that YOLOv8 was the most suitable model for our application, providing an optimal balance between performance, ease of deployment, and generalization capabilities without the need to experiment with more complex architectures like Dual Attention CNNs (DAC) [39] or ViTs [36].

2.8 Brain Tumor Classification

This section covers the second phase of the proposed pipeline, the brain tumor classification step. In this step, the Knowledge Distillation (KD) technique is deployed to train a lightweight ViT from the ResNet152 model on our classification dataset (Figure 4).

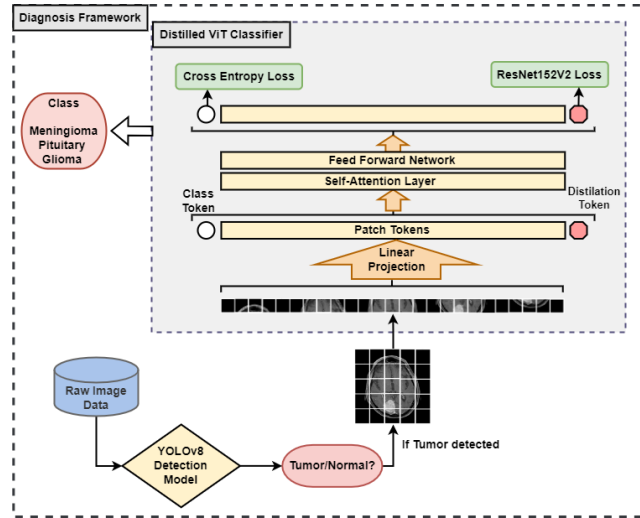


Fig. 4. The proposed framework for brain tumor classification.

KD [40], is a training method in which a less powerful student model learns from the guidance of a more capable teacher network. Unlike traditional training, where only the teacher's highest-scoring outputs (hard labels) are considered, KD uses the complete output vector generated by the teacher's Softmax function. This approach not only enhances the performance of the student model but can also be seen as a way of compressing the knowledge contained in the larger teacher model into a smaller,

more efficient student model. In the context of KD, following up on the further advancement of computer vision, DeiT [12] marks a significant stride by initially applying the KD technique to ViT, aimed at distilling valuable insights from CNNs to enhance training efficiency.

2.9 Justification for Choosing DeiT as the Backbone

In this study, the DeiT model was selected as the backbone for the classification phase due to several important factors that make it particularly suitable for our use case. One key reason is DeiT's effectiveness in scenarios where data availability is limited, which is often the case in medical imaging datasets. Compared to traditional ViTs, DeiT is specifically designed to achieve high performance with smaller datasets by utilizing KD from larger models, thus striking an efficient balance between model size and accuracy.

DeiT also provides practical advantages for deployment in medical settings where computational resources might be constrained. Other potential backbones, such as larger CNN-based architectures (e.g., EfficientNet, DenseNet) or even more complex ViTs, while potentially more accurate, often come at the cost of higher computational demand. These architectures typically require large-scale datasets to reach their full potential, which might not align well with the resource-limited medical environments.

Additionally, the KD technique employed by DeiT allows it to leverage the strengths of a more computationally expensive ResNet152 teacher model while retaining the lightweight and efficient nature of a transformer-based student model. This reduces both training time and inference costs without compromising significantly on performance.

Finally, DeiT's ability to handle image data with intricate details, such as brain tumor classification across different tumor types, makes it a versatile and robust solution for this particular task. For future works, however, exploring other cutting-edge transformers or CNN backbones remains an intriguing possibility.

2.10 ResNet-152

ResNet-152, Residual Network with 152 layers, is a significant deep CNN architecture primarily tailored for image classification and feature extraction tasks. It belongs to the ResNet model family, is widely recognized for its outstanding performance in computer vision applications, and represents an improved iteration of the original ResNet-152. A notable innovation within ResNet models is the inclusion of residual blocks, which effectively address the challenge of vanishing gradients when training deep neural networks (DNN). The "vanishing gradients" problem in DNN occurs when gradients become too small during training, hindering the learning process of the model.

2.11 Vision Transformer

One of the main components of our pipeline is ViT. This model [36] works by treating pieces of an image like words in a sentence, trying to mimic how the original transformer model was used for

understanding language [41]. Unlike the original transformer, which had both an encoder and a decoder, ViT keeps things more straightforward with just an encoder in its design. In ViT, the input image has dimensions $R^{H \times W \times C}$. It's then split into N smaller pieces called patches, each sized at $P \times P \times C$, where $N = \frac{HW}{p^2}$ [30].

Next, the model creates a linear representation for these patches and adds position information to these representations to know where each patch is located. Additionally, an additional patch is included in the embedding that can be adjusted through learning. This embedding is used for the final classification step and is processed by a multi-layer Perceptron (MLP) head. Moreover, the combined information from the patches and their position embeddings are taken and passed through a transformer encoder model. This encoder model consists of multiple layers that alternate between multi-headed self-attention and MLP blocks.

2.12 Evaluation Metrics

Upon completing the training and testing phases, it is imperative to employ standardized assessment criteria to evaluate the model's effectiveness. In recent studies, the researchers utilized a range of evaluation metrics, including Precision, Recall, Sensitivity, Specificity, Accuracy, F1-score. These metrics are derived by applying the model to the data set and tallying the occurrences of True Positives (TP), True Negatives (TN), False Positives (FP), and False Negatives (FN). TP denotes instances where the model accurately identified and labeled tumor cases, while FP refers to non-tumor cases incorrectly classified as tumors. FN represents tumors that went unrecognized during the diagnostic process. TN signifies true negatives, where the model's predictions are aligned with the actual negative cases. As for the classification phase, we utilized a diverse range of evaluation metrics to clearly observe the model's performance. It is critical to mention that the PTP evaluation metrics are only employed in the tumor detection phase exclusively.

$$Precision = TP / (TP + FP)$$

$$Recall = TP / (TP + FN)$$

Notably, the F1-score, which computes the harmonic mean between Precision and Recall, is frequently regarded as a primary metric for evaluating model performance in situations where data sets exhibit an imbalance in class distribution.

$$F1_Score = 2 \times (Precision \times Recall) / (Precision + Recall)$$

2.13 Classification Dataset

During the classification phase, we accurately combined two datasets (www.kaggle.com/datasets/masoudnickparvar/brain-tumor-mri-dataset, accessed on August 2023 and Figshare dataset [42]) for our training and validation sets and also divided a set for benchmarking the model. To diversify and increase the number of samples per class, we took similar to detection phase data pre-processing steps.

2.14 Computational Resources

We primarily utilized a local system with a single CUDA-enabled Nvidia GeForce GTX 1650 GPU. On occasion, we also used Google Colab, which provided 12 GB of RAM and a T4 GPU. For model training, validation, and testing, we employed PyTorch version 2.0.1+cu117 with Python 3.9.7. We deployed the ViT model using the P Wang GitHub repository [43] implementation, while the ResNet152 model was trained and evaluated using the Torch Vision models module.

3. Results

In this section, we will elaborate on the experiments and the results we achieved from deploying the proposed pipeline. First, we are going to explain the detection phase results, and then we will transition to the next stage, which is classification.

3.1 Detection Results

The initial step in this phase was data pre-processing. After conducting a comprehensive data preparation and transforming the data set into a suitable format, we loaded the YOLOv8n model pre-trained weights, tailored its hyper-parameters and fine-tuned it on our detection dataset. For this phase, we used the dataset we acquired from NBML for both the training and validation steps.

In first training attempt we ended up with a precise model with low recall score as we were inducing unwanted misinformation into the model's learning path. The bounding boxes that we specified for tumor regions were accurate in the majority of the augmentations including the vertical and horizontal flips.

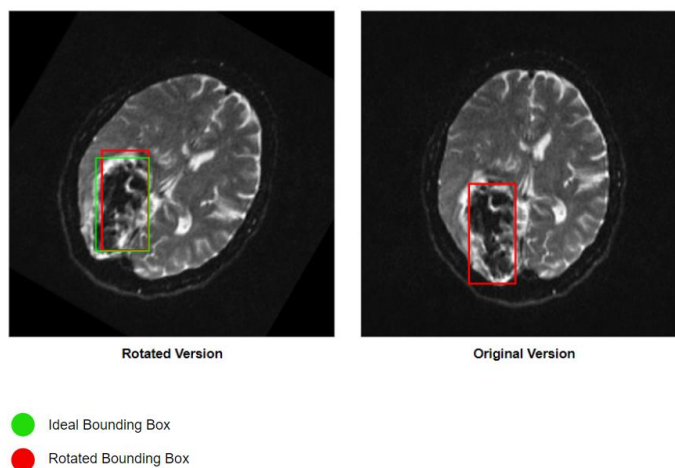


Fig. 5. The rotation of bounding boxes has a notable impact on our models, affecting their ability to accurately outline objects by introducing misleading information within the boxed area. The extent of this inaccuracy depends on the tumor's shape, size, and how much it is rotated.

However, the rotation of the image and the corresponding object of interest (Tumor) was injecting false information into the Tumor class. This happened when we attempted to rotate the bounding box around its initial center using our custom module, and some non-tumor regions were injected in the

new bounding box region. Therefore, we decided to stay with more reliable augmentation effects such as vertical, horizontal flips and brightness intensity.

Table. 1. YOLOV8N MODEL VALIDATION BOX RESULTS OVER 40 EPOCHS

| Data | Precision | Recall | mAP50 |
|-------------------------|-----------|--------|-------|
| With-Rotated Samples | 0.74 | 0.58 | 0.68 |
| Without-Rotated Samples | 0.87 | 0.71 | 0.80 |

Furthermore, in consideration of our constrained access to computational resources, we opted for the most compact iteration of YOLOv8, denoted as Nano. We employed larger batch sizes to expedite the training duration per epoch. The consideration of employing advanced versions of YOLOv8, such as YOLOv8m or YOLOv8L, suggests the possibility of achieving improved results. Nevertheless, it is important to acknowledge that this choice comes with the trade-off of extended training periods and increased demands on computational resources.

Table. 2. YOLOV8N MODEL CONFIGURATION

| Opt | Sched | lr0 | lrf | AMP | Epochs |
|-----|-------|------|---------|-------|--------|
| SGD | CosLR | 0.01 | 0.00001 | False | 40 |

Opt: Optimizer, Sched: Scheduler, lr0: Initial learning rate, lrf: Final learning rate, AMP: Automatic Mixed Precision

Table. 3. YOLOV8N MODEL EVALUATION RESULTS

| Class | Precision | Recall | F1 | Support |
|------------|-----------|--------|------|---------|
| Tumor | 0.99 | 0.96 | 0.97 | 1905 |
| Normal | 0.99 | 0.99 | 0.99 | 20750 |
| AVG | 0.99 | 0.975 | 0.98 | 22655 |

We trained the mentioned model for 40 epochs, and the evaluation results indicated (Table III) that the model is highly accurate in detecting tumor-confiscated images, and despite being agile and super lightweight with only 3.2M parameters, it does have a reliable performance.

Table. 4. YOLOV8N MODEL PTP EVALUATION RESULTS

| Support | Accuracy | F1 | Precision | Recall |
|--------------------|----------|-----|-----------|--------|
| 3 Tumor Patients | 1.0 | 1.0 | 1.0 | 1.0 |
| 27 Normal Patients | 1.0 | 1.0 | 1.0 | 1.0 |

Furthermore, the model manages to achieve significant scores in our PTP evaluation, as detailed in Table IV. The value of GTT is the output of a meticulous data analysis step in our training and evaluation sets. We incorporated the training and validation sets in their original format into the model and calculated the value of GTT for each patient of these sets. After an exploratory analysis of the patient specific tumor threshold (Figure 6) values among the both Normal and Tumor cases, we estimated the value of the GTT to be at least be 0.04%. This value is calculated from the average of the first quartile and the median values of tumor-indicative distribution.

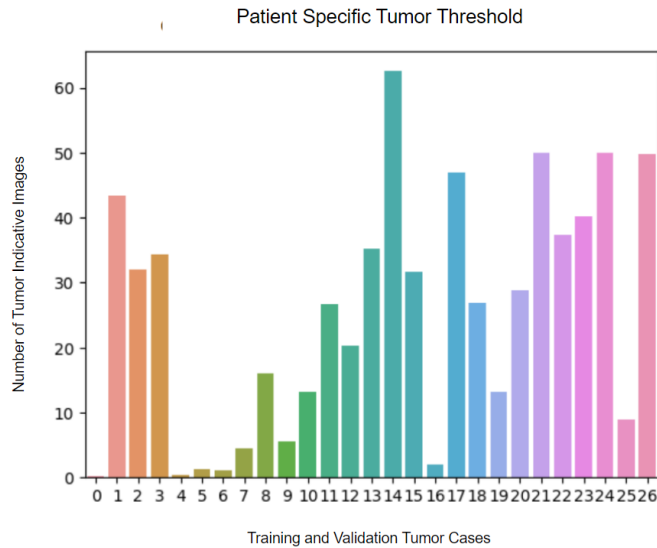


Fig. 6. Patient Specific Tumor Threshold, computed for each patient, represents the proportion of images depicting tumors within the entire image set for that patient.

The performance of our detection model, as demonstrated in Fig. 7, provides a clear indication of its robustness. Throughout training, the validation metrics show consistent improvement, while the training loss decreases steadily. This parallel progression between training and validation suggests a well-balanced model that is neither underfitting nor overfitting. Typically, overfitting manifests as a divergence between training and validation results—where training loss decreases but validation performance plateaus or worsens. However, the steady improvement in both metrics, as observed in Fig. 7, confirms the model's ability to generalize effectively to new data.

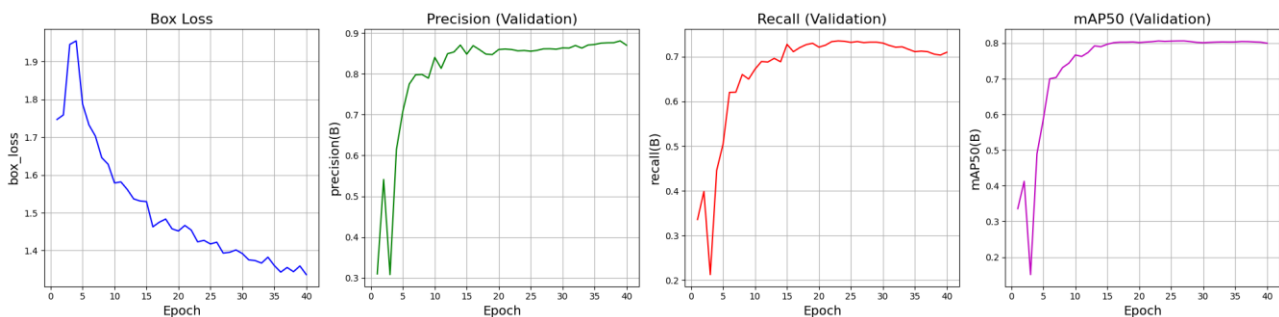


Fig. 7. Validation Performance Metrics and Training Loss Over Epochs for the YOLOv8n Detection Model.

The detection model achieved an impressive F1-Score of 0.98 and Precision of 0.99, even in a highly imbalanced dataset designed to reflect real-world clinical scenarios, where tumor cases are rare. This performance is further supported by the use of carefully designed data preprocessing and augmentation techniques that increase the diversity of the training samples while maintaining the integrity of the anomaly distribution. By skewing the dataset toward a low-incidence tumor rate, the model was exposed to a challenging yet realistic detection environment, which further validates its ability to handle rare-event scenarios.

Moreover, the introduction of the Patient-to-Patient (PTP) evaluation framework, which assesses model performance at the patient level, reinforces the clinical relevance of the results. The PTP metric captures how well the model identifies tumor patients in an imbalanced population, ensuring that the

model performs effectively not just on individual images but across entire patient datasets, aligning with real-world diagnostic needs.

3.2 Classification Results

The approach we took for this phase is based on knowledge distillation (KD) using the DeiT architecture. Initially, we created a relatively large dataset from the training set, which was obtained from the Figshare dataset, and applied our custom data augmentation module to increase the diversity of the samples. Following this, we fine-tuned a strong teacher model using the ResNet152 architecture, known for its robust feature extraction capabilities in image classification tasks.

During the distillation process, having access to a strong teacher model is crucial. In our case, the ResNet152 model served as the teacher, leveraging its deep convolutional neural network (CNN) kernels to capture complex features and patterns. These rich features were then transferred to the DeiT student model, allowing it to be trained efficiently from scratch. The benefit of the DeiT architecture lies in its ability to produce compact ViT models distilled from larger, more computationally expensive teacher models. This process is particularly useful when working with limited datasets, as is common in medical imaging applications.

Table 5. DEIT HYPER-PARAMETERS TUNING EXPERIMENTS

| NO | Hard Distillation | Temperature | Depth | Patch Size | Dimension | Attention Head | MLP Dim | Val-Accuracy |
|----|-------------------|-------------|-------------|--------------|---------------|----------------|---------------|--------------|
| 1 | False (Default) | 2 (Default) | 4 (Default) | 24 (Default) | 256 (Default) | 16 (Default) | 128 (Default) | 81.91 |
| 2 | True | 2 (Default) | 4 (Default) | 24 (Default) | 256 (Default) | 16 (Default) | 128 (Default) | 84.74 |
| 3 | True | 1 | 4 (Default) | 24 (Default) | 256 (Default) | 16 (Default) | 128 (Default) | 83.22 |
| 4 | True | 9 | 4 (Default) | 24 (Default) | 256 (Default) | 16 (Default) | 128 (Default) | 81.69 |
| 5 | True | 3 | 6 | 24 (Default) | 256 (Default) | 16 (Default) | 128 (Default) | 82.35 |
| 6 | True | 3 | 2 | 32 | 256 (Default) | 16 (Default) | 128 (Default) | 85.40 |
| 7 | True | 3 | 2 | 24 | 256 (Default) | 16 (Default) | 128 (Default) | 86.05 |
| 8 | True | 3 | 2 | 24 | 1024 | 16 (Default) | 128 (Default) | 68.19 |
| 9 | True | 3 | 2 | 24 | 128 | 16 (Default) | 128 (Default) | 85.40 |
| 10 | True | 3 | 2 | 24 | 512 | 16 (Default) | 128 (Default) | 74.29 |
| 11 | True | 3 | 2 | 24 | 128 | 64 | 128 (Default) | 88.67 |
| 12 | True | 3 | 2 | 24 | 128 | 64 | 256 | 88.45 |
| 13 | True | 3 | 2 | 24 | 128 | 64 | 2048 | 87.58 |
| 14 | True | 3 | 2 | 24 | 128 | 64 | 512 | 89.76 |

We proceeded to tune the hyperparameters of the DeiT model by exploring 14 different architectural variations to find the optimal settings. The specifics of these experiments are detailed in Table V. After

finalizing the model architecture, we evaluated the DeiT model’s performance on a dataset of 1,600 training images, 400 validation images, and 400 test images, which consisted of three classes of brain tumors: Meningioma, Glioma, and Pituitary.

The DeiT student model performed well across all classes, particularly excelling in classifying the Pituitary tumor class, with an F1-Score of 0.97. For Glioma, the model achieved an F1-Score of 0.93, while Meningioma classification resulted in a slightly lower F1-Score of 0.82. The weighted average F1-Score across all three classes was 0.92. These results demonstrate the model’s effectiveness in learning the distinguishing features of each tumor type, despite the relatively small size of the dataset and the limited number of training epochs.

While the DeiT student model achieved a slightly lower F1-Score of 0.92 compared to the ResNet152 teacher model’s F1-Score of 0.97, this difference can be attributed to several factors. Firstly, the ResNet teacher model was trained on a heavily augmented dataset, using our custom data augmentation module to generate a wide variety of image variations. This allowed the teacher model to generalize better and capture more nuanced features. However, this process also increased the computational cost of training the ResNet model, making it less practical for real-time applications.

Table. 6. TEACHER CLASSIFIER TEST RESULTS

| Tumor Class | Precision | Recall | F1 | Support |
|---------------------|------------------|---------------|-------------|----------------|
| Meningioma | 0.92 | 0.91 | 0.91 | 107 |
| Glioma | 0.99 | 0.97 | 0.98 | 214 |
| Pituitary | 0.94 | 0.97 | 0.96 | 140 |
| Weighted AVG | 0.97 | 0.97 | 0.97 | 461 |

Table. 7. DISTILLED STUDENT CLASSIFIER TEST RESULTS

| Tumor Class | Precision | Recall | F1 | Support |
|---------------------|------------------|---------------|-------------|----------------|
| Meningioma | 0.82 | 0.82 | 0.82 | 107 |
| Glioma | 0.95 | 0.97 | 0.93 | 214 |
| Pituitary | 0.95 | 0.99 | 0.96 | 140 |
| Weighted AVG | 0.92 | 0.97 | 0.97 | 461 |

In contrast, the DeiT student model was trained for only 20 epochs with fewer computational resources. Despite these constraints, the DeiT model demonstrated competitive performance, showing its potential as a lightweight and efficient alternative for medical applications, where computational resources and data availability are often limited. The DeiT model’s ability to maintain high performance under these conditions highlights its suitability for deployment in resource-constrained environments, providing a good trade-off between accuracy and efficiency.

To ensure fairness in the evaluation process, we used the same testing dataset for both the teacher (ResNet) and student (DeiT) models, with 15% of the original dataset specifically allocated for benchmarking. However, during the training phase, the ResNet teacher model was trained on an augmented dataset, incorporating various transformations to improve generalization, while the DeiT student model was trained on a non-augmented dataset. This difference in training conditions explains

part of the performance gap between the two models. Despite the absence of data augmentation during training, the DeiT model still performed competitively on the same testing dataset, showcasing its efficiency. This result confirms the hypothesis that DeiT is more efficient and better suited to data-scarce situations compared to heavier networks like ResNet, making it a strong candidate for real-world applications where data and computational resources are often limited.

4. Discussion and conclusions

This study presents a comprehensive evaluation of state-of-the-art models, specifically YOLOv8 and DeiT, for the detection and classification of brain tumors from medical imaging data. A key contribution of this work lies in the introduction of novel performance metrics, particularly the PTP evaluation framework. These metrics are designed not only to assess the models' efficacy in detecting and classifying brain tumors but also to provide a more clinically relevant evaluation by considering the patient's overall condition rather than individual images in isolation.

- Unique Data Preprocessing and Distribution:

To ensure a realistic simulation of clinical settings, we curated a dataset comprising both Tumor and Normal cases, carefully maintaining an imbalanced distribution with only 10% of cases representing tumors. This distribution reflects real-world medical scenarios, where tumor incidence rates are low. Unlike prior studies, which often rely on semi-balanced datasets, our approach to data preprocessing was specifically designed to mirror the challenges posed by clinical anomaly detection. Consequently, direct comparisons with previous works are inherently difficult, as they typically operate under more balanced conditions that do not align with the rare-event scenario modeled in this study.

- Novel Patient-to-Patient (PTP) Metric:

The detection phase results, evaluated using both conventional metrics and the newly introduced PTP metric, demonstrate the robustness of the proposed models. Achieving an F1-Score of 0.98 and a perfect PTP-F1 score of 1.0 in challenging, imbalanced scenarios highlights the system's accuracy. The PTP metric offers a patient-centered perspective, evaluating the model's ability to make accurate diagnoses across multiple images from a single patient. This patient-level evaluation framework is particularly relevant in clinical practice, where diagnosis is not made on an image-by-image basis. However, this novel evaluation method makes direct comparisons with other studies problematic, as most existing works are evaluated at the image level and do not provide the comprehensive, patient-centric evaluation necessary in real-world medical applications.

- Dataset Limitations and Benchmark Comparisons:

The final phase of our study employed the DeiT architecture, where a lightweight ViT model was distilled from a ResNet152-based teacher model. Despite training for a limited number of epochs, the student model achieved a commendable test accuracy of 0.92. However, it is important to note that our results in the classification phase were evaluated using standard metrics rather than the PTP metric, as the latter is specifically designed for the detection phase. The extension of PTP-like metrics to classification tasks remains an area for potential future investigation.

A key challenge in comparing our results to previous studies is the nature of publicly available benchmark datasets. For instance, the Figshare dataset lacks patient-specific labels and presents data

in a shuffled format. In contrast, our dataset from the NBML includes patient-level annotations, providing a more clinically relevant evaluation. This distinction highlights the unique value of our approach, as existing studies generally do not use a patient-centered evaluation methodology. Future research can build on this by developing datasets with patient-specific annotations to further enhance comparisons and validation of patient-level metrics.

In conclusion, this study introduces a novel approach to detect and classify brain tumors in anomalous populations. However, further refinement of the GTT and broader application of the PTP metric to other clinical conditions are suggested. Integrating patient-level evaluation frameworks into larger datasets will also enhance benchmarking and enable more robust comparative analyses.

5. Data Statement

This research has been conducted using the IBMB resources. The IBMB resources including the NBML tumor detection dataset, are available for approved projects from <http://ibmb.nbml.ir>.

6. Funding Sources

This research received no specific grant from funding agencies in the public, commercial, or not-for-profit sectors.

Declaration of competing interest

The authors declare that they have no known competing financial interests or personal relationships that could have appeared to influence the work reported in this paper.

Appendix A. Supplementary data

A preliminary version of this research article was made available on arXiv [44].

Acknowledgments

We would like to thank Dr. Mohammad Reza Ay, director of NBML for sharing the brain tumor detection dataset.

References

- [1] D.N. Louis, A. Perry, G. Reifenberger, A. von Deimling, D. Figarella-Branger, W.K. Cavenee, H. Ohgaki, O.D. Wiestler, P. Kleihues, D.W. Ellison, The 2016 World Health Organization

Classification of Tumors of the Central Nervous System: a summary, *Acta Neuropathol* 131 (2016). <https://doi.org/10.1007/s00401-016-1545-1>.

- [2] G.S. Tandel, M. Biswas, O.G. Kakde, A. Tiwari, H.S. Suri, M. Turk, J.R. Laird, C.K. Asare, A.A. Ankrah, N.N. Khanna, B.K. Madhusudhan, L. Saba, J.S. Suri, A review on a deep learning perspective in brain cancer classification, *Cancers (Basel)* 11 (2019). <https://doi.org/10.3390/cancers11010111>.
- [3] A. Kabir Anaraki, M. Ayati, F. Kazemi, Magnetic resonance imaging-based brain tumor grades classification and grading via convolutional neural networks and genetic algorithms, *Biocybern Biomed Eng* 39 (2019). <https://doi.org/10.1016/j.bbe.2018.10.004>.
- [4] R. Augustine, A. Al Mamun, A. Hasan, S.A. Salam, R. Chandrasekaran, R. Ahmed, A.S. Thakor, Imaging cancer cells with nanostructures: Prospects of nanotechnology driven non-invasive cancer diagnosis, *Adv Colloid Interface Sci* 294 (2021). <https://doi.org/10.1016/j.cis.2021.102457>.
- [5] K. Popuri, D. Cobzas, A. Murtha, M. Jägersand, 3D variational brain tumor segmentation using Dirichlet priors on a clustered feature set, *Int J Comput Assist Radiol Surg* 7 (2012). <https://doi.org/10.1007/s11548-011-0649-2>.
- [6] "Brain Tumors and Brain Cancer," <https://www.hopkinsmedicine.org/health/conditions-and-diseases/brain-tumor> (n.d.). <https://www.hopkinsmedicine.org/health/conditions-and-diseases/brain-tumor> (accessed August 31, 2023).
- [7] J. Kang, Z. Ullah, J. Gwak, Mri-based brain tumor classification using ensemble of deep features and machine learning classifiers, *Sensors* 21 (2021). <https://doi.org/10.3390/s21062222>.
- [8] K. Simonyan, A. Zisserman, Very deep convolutional networks for large-scale image recognition, in: *3rd International Conference on Learning Representations, ICLR 2015 - Conference Track Proceedings*, 2015.
- [9] C. Szegedy, W. Liu, Y. Jia, P. Sermanet, S. Reed, D. Anguelov, D. Erhan, V. Vanhoucke, A. Rabinovich, Going deeper with convolutions, in: *Proceedings of the IEEE Computer Society Conference on Computer Vision and Pattern Recognition*, 2015. <https://doi.org/10.1109/CVPR.2015.7298594>.
- [10] K. He, X. Zhang, S. Ren, J. Sun, Deep residual learning for image recognition, in: *Proceedings of the IEEE Computer Society Conference on Computer Vision and Pattern Recognition*, 2016. <https://doi.org/10.1109/CVPR.2016.90>.
- [11] "Key Statistics for Brain and Spinal Cord Tumors," <https://www.cancer.org/cancer/types/brain-spinal-cord-tumors-adults/about/key-statistics.html> (n.d.). <https://www.cancer.org/cancer/types/brain-spinal-cord-tumors-adults/about/key-statistics.html> (accessed August 31, 2023).
- [12] H. Touvron, M. Cord, M. Douze, F. Massa, A. Sablayrolles, H. Jégou, Training data-efficient image transformers & distillation through attention, in: *Proc Mach Learn Res*, 2021.

- [13] K. Kavin Kumar, T. Meera Devi, S. Maheswaran, An efficient method for brain tumor detection using texture features and SVM classifier in MR images, *Asian Pacific Journal of Cancer Prevention* 19 (2018). <https://doi.org/10.22034/APJCP.2018.19.10.2789>.
- [14] E.I. Zacharaki, S. Wang, S. Chawla, D.S. Yoo, R. Wolf, E.R. Melhem, C. Davatzikos, Classification of brain tumor type and grade using MRI texture and shape in a machine learning scheme, *Magn Reson Med* 62 (2009). <https://doi.org/10.1002/mrm.22147>.
- [15] S. Shrot, M. Salhov, N. Dvorski, E. Konen, A. Averbuch, C. Hoffmann, Application of MR morphologic, diffusion tensor, and perfusion imaging in the classification of brain tumors using machine learning scheme, *Neuroradiology* 61 (2019). <https://doi.org/10.1007/s00234-019-02195-z>.
- [16] S. Deepak, P.M. Ameer, Retrieval of brain MRI with tumor using contrastive loss based similarity on GoogLeNet encodings, *Comput Biol Med* 125 (2020). <https://doi.org/10.1016/j.compbiomed.2020.103993>.
- [17] Z.N.K. Swati, Q. Zhao, M. Kabir, F. Ali, Z. Ali, S. Ahmed, J. Lu, Brain tumor classification for MR images using transfer learning and fine-tuning, *Computerized Medical Imaging and Graphics* 75 (2019). <https://doi.org/10.1016/j.compmedimag.2019.05.001>.
- [18] Y. Zhuge, H. Ning, P. Mathen, J.Y. Cheng, A. V. Krauze, K. Camphausen, R.W. Miller, Automated glioma grading on conventional MRI images using deep convolutional neural networks, *Med Phys* 47 (2020). <https://doi.org/10.1002/mp.14168>.
- [19] R. Pomponio, G. Erus, M. Habes, J. Doshi, D. Srinivasan, E. Mamourian, V. Bashyam, I.M. Nasrallah, T.D. Satterthwaite, Y. Fan, L.J. Launer, C.L. Masters, P. Maruff, C. Zhuo, H. Völzke, S.C. Johnson, J. Fripp, N. Koutsouleris, D.H. Wolf, R. Gur, R. Gur, J. Morris, M.S. Albert, H.J. Grabe, S.M. Resnick, R.N. Bryan, D.A. Wolk, R.T. Shinohara, H. Shou, C. Davatzikos, Harmonization of large MRI datasets for the analysis of brain imaging patterns throughout the lifespan, *Neuroimage* 208 (2020). <https://doi.org/10.1016/j.neuroimage.2019.116450>.
- [20] M.A. Naser, M.J. Deen, Brain tumor segmentation and grading of lower-grade glioma using deep learning in MRI images, *Comput Biol Med* 121 (2020). <https://doi.org/10.1016/j.compbiomed.2020.103758>.
- [21] Ö. Polat, C. Güngen, Classification of brain tumors from MR images using deep transfer learning, *Journal of Supercomputing* 77 (2021). <https://doi.org/10.1007/s11227-020-03572-9>.
- [22] H.A. Khan, W. Jue, M. Mushtaq, M.U. Mushtaq, Brain tumor classification in MRI image using convolutional neural network, *Mathematical Biosciences and Engineering* 17 (2020). <https://doi.org/10.3934/MBE.2020328>.
- [23] M.M. Badža, M.C. Barjaktarović, Classification of brain tumors from mri images using a convolutional neural network, *Applied Sciences (Switzerland)* 10 (2020). <https://doi.org/10.3390/app10061999>.
- [24] E.U. Haq, H. Jianjun, K. Li, H.U. Haq, T. Zhang, An MRI-based deep learning approach for efficient classification of brain tumors, *J Ambient Intell Humaniz Comput* 14 (2023). <https://doi.org/10.1007/s12652-021-03535-9>.

- [25] A. Sekhar, S. Biswas, R. Hazra, A.K. Sunaniya, A. Mukherjee, L. Yang, Brain Tumor Classification Using Fine-Tuned GoogLeNet Features and Machine Learning Algorithms: IoMT Enabled CAD System, *IEEE J Biomed Health Inform* 26 (2022). <https://doi.org/10.1109/JBHI.2021.3100758>.
- [26] N.S. Shaik, T.K. Cherukuri, Multi-level attention network: application to brain tumor classification, *Signal Image Video Process* 16 (2022). <https://doi.org/10.1007/s11760-021-02022-0>.
- [27] M.F. Alanazi, M.U. Ali, S.J. Hussain, A. Zafar, M. Mohatram, M. Irfan, R. Alruwaili, M. Alruwaili, N.H. Ali, A.M. Albarrak, Brain Tumor/Mass Classification Framework Using Magnetic-Resonance-Imaging-Based Isolated and Developed Transfer Deep-Learning Model, *Sensors* 22 (2022). <https://doi.org/10.3390/s22010372>.
- [28] B. Ahmad, J. Sun, Q. You, V. Palade, Z. Mao, Brain Tumor Classification Using a Combination of Variational Autoencoders and Generative Adversarial Networks, *Biomedicines* 10 (2022). <https://doi.org/10.3390/biomedicines10020223>.
- [29] M.I. Sharif, M.A. Khan, M. Alhussein, K. Aurangzeb, M. Raza, A decision support system for multimodal brain tumor classification using deep learning, *Complex and Intelligent Systems* 8 (2022). <https://doi.org/10.1007/s40747-021-00321-0>.
- [30] A.A. Asiri, A. Shaf, T. Ali, U. Shakeel, M. Irfan, K.M. Mehdar, H.T. Halawani, A.H. Alghamdi, A.F.A. Alshamrani, S.M. Alqhtani, Exploring the Power of Deep Learning: Fine-Tuned Vision Transformer for Accurate and Efficient Brain Tumor Detection in MRI Scans, *Diagnostics* 13 (2023). <https://doi.org/10.3390/diagnostics13122094>.
- [31] S. Tummala, S. Kadry, S.A.C. Bukhari, H.T. Rauf, Classification of Brain Tumor from Magnetic Resonance Imaging Using Vision Transformers Ensembling, *Current Oncology* 29 (2022). <https://doi.org/10.3390/curroncol29100590>.
- [32] A.B. Abdusalomov, M. Mukhiddinov, T.K. Whangbo, Brain Tumor Detection Based on Deep Learning Approaches and Magnetic Resonance Imaging, *Cancers (Basel)* 15 (2023). <https://doi.org/10.3390/cancers15164172>.
- [33] J.A. Cruz, D.S. Wishart, Brain and Other Nervous System Cancer — Cancer Stat Facts, *National Cancer Institute* 2 (2019).
- [34] J. Solawetz, Francesco, What is YOLOv8? The Ultimate Guide., *Roboflow* (2023).
- [35] M.G. Ragab, S.J. Abdulkadir, A. Muneer, A. Alqushaibi, E.H. Sumiea, R. Qureshi, S.M. Al-Selwi, H. Alhussian, A Comprehensive Systematic Review of YOLO for Medical Object Detection (2018 to 2023), *IEEE Access* 12 (2024). <https://doi.org/10.1109/ACCESS.2024.3386826>.
- [36] A. Dosovitskiy, L. Beyer, A. Kolesnikov, D. Weissenborn, X. Zhai, T. Unterthiner, M. Dehghani, M. Minderer, G. Heigold, S. Gelly, J. Uszkoreit, N. Houlsby, AN IMAGE IS WORTH 16X16 WORDS: TRANSFORMERS FOR IMAGE RECOGNITION AT SCALE, in: *ICLR 2021 - 9th International Conference on Learning Representations*, 2021.
- [37] A. Bochkovskiy, H. Yuan Mark Liao, YOLOv4: Optimal Speed and Accuracy of Object Detection, *CoRR abs/2004.10934* (2020).

- [38] Brief summary of YOLOv8 model structure,
<https://Github.Com/Ultralytics/Ultralytics/Issues/189> (n.d.).
<https://github.com/ultralytics/ultralytics/issues/189> (accessed August 31, 2023).
- [39] J. Fu, J. Liu, H. Tian, Y. Li, Y. Bao, Z. Fang, H. Lu, Dual attention network for scene segmentation, in: Proceedings of the IEEE Computer Society Conference on Computer Vision and Pattern Recognition, 2019. <https://doi.org/10.1109/CVPR.2019.00326>.
- [40] G. Hinton, O. Vinyals, J. Dean, Distilling the knowledge in a neural network, ArXiv Preprint ArXiv:1503.02531 (2015).
- [41] A. Vaswani, N. Shazeer, N. Parmar, J. Uszkoreit, L. Jones, A.N. Gomez, Ł. Kaiser, I. Polosukhin, Attention is all you need, in: Adv Neural Inf Process Syst, 2017.
- [42] J. Cheng, brain tumor dataset, Figshare (2017).
- [43] P. Wang, vit-pytorch, (n.d.).
- [44] S.M.H. Hashemi, L. Safari, A. Dadashzadeh Taromi, Realism in Action: Anomaly-Aware Diagnosis of Brain Tumors from Medical Images Using YOLOv8 and DeiT, ArXiv Preprint ArXiv:2401.03302 (2024).